Two-Layer Quasigeostrophic Flow over Finite Isolated Topography

LUANNE THOMPSON

School of Oceanography, University of Washington, Seattle, Washington

(Manuscript received 26 December 1991, in final form 11 June 1992)

ABSTRACT

A quasigeostrophic two-layer model of flow over finite topography is developed. The topography is a right circular cylinder that extends through the lower layer and an order Rossby number amount into the upper layer (finite topography model). Thus, each layer depth remains constant to first order, and the quasigeostrophic approximation can be applied consistently. The model solutions are compared to those found when the total topographic height is order Rossby number (small topography model). The steady solution for the finite topography model consists of two parts: one similar to the small topography solution and forced by the anticyclonic potential vorticity anomaly over the topography and the other similar to the solution of potential flow around a cylinder and forced by the matching conditions on the edge of the topography. The finite topography model breaks down when the interface goes above the topography. This occurs most easily when the stratification is weak. Closed streamlines occur more readily over the topography when the stratification is weak, opposite to the tendency of the small topography model. The initial value problem is studied in both two-layer geometries. A modified contour dynamics method is developed to apply the boundary and matching conditions on the edge of the topography in the finite topography model. In the small topography model, an eddy is shed that is cyclonic, warm core, and bottom trapped; while the shed eddy is cyclonic, cold core, and surface intensified in the finite topography model.

1. Introduction

Seamounts in the ocean often reach nearly to the surface and affect the flow of ocean currents throughout the water column. For instance, Vastano and Warren (1976) report observations near the Atlantis II Seamount, which rises within 1645 m of the surface of the ocean, over 3000 m from the bottom. Below the top of the seamount, lines of constant potential temperature (which we interpret loosely as streamlines) split around the seamount, while in the upper levels, some fluid moves over the seamount and isotherms are deflected to the left (looking downstream) of the seamount. Because the topography was so tall, quasigeostrophic dynamics are not useful in interpretation of these observations. Even with a small hill [for example, see Gould et al. (1981) who studied flow near a 500-m seamount] the rise of the isotherms is not as high as would be expected from quasigeostrophic theory, indicating that the finite nature of the topography (although it was only 0.1 times the total depth of the water) caused the flow to go around the topography at the lowest levels.

Steady inviscid solutions of flow over topography have been found previously by using the quasigeostrophic approximation, including the effect of stratification and β (for instance, see Hogg 1973; McCartney 1975; Janowitz 1975; Johnson 1977, 1979). The more oceanographically realistic situation with topography of finite height has also been considered with inviscid models, although study has been limited to situations in which the bottom boundary remains an isopycnal surface (Merkine and Kalnay-Rivas 1976). This is an unsatisfactory approximation when flow interacts with tall seamounts and isopycnals intersect the topography.

Buzzi and Speranza (1979) explore the limitations of quasigeostrophic theory by studying the difference between two classes of solutions in a continuously stratified model: one where the topography has height (h_0) proportional to the Rossby number (ϵ), and the other where the topography has finite height. They argue that when the stratification is weak or the topography is small, the flow can go up and over the obstacle; when the topography is tall or the stratification strong, the flow must go around the obstacle in order to keep the flow quasi-horizontal as required by quasigeostrophic theory. First, they consider flow over a hemispherical obstacle. This solution is similar to other quasigeostrophic solutions found in a stratified fluid, and in the far field the velocity falls off as r^{-1}. The solution is found by applying the impenetrability condition to the vertical velocity at the bottom. They then consider flow past a half disk standing vertically in the fluid. In this case, the topography acts like a vertical wall, and the impenetrability condition is applied on the horizontal velocity; the streamfunction at the wall

Corresponding author address: Dr. LuAnne Thompson, School of Oceanography, WB-10, University of Washington, Seattle, WA 98195.

depends only on the vertical coordinate and is specified arbitrarily. The velocity in the far field falls off as r^{-2}, and the flow goes entirely around the obstacle. One might expect that in a general stratified model with flow over topography with finite vertical and horizontal cross section, the solutions would contain elements of the two types of solutions that they discuss. Ou (1991) has also considered quasigeostrophic flow over a finite height obstacle to look at the transition from partial blocking of the fluid by the obstacle to total blocking of the fluid. He used a two-layer model and used frictional effects to tie the two dynamical regimes together.

Steady solutions give useful insight into important dynamical processes, but we would also like to consider how the steady solutions are related to the initial value problem and time-dependent situations. There have been several approaches to the study of the initial value problem, using both finite-difference methods and contour dynamics. Huppert and Bryan (1976) solve for flow over topography in a periodic domain using a primitive equation model with continuous stratification. They demonstrate two different flow regimes: one in which the fluid originated over the topography and is trapped there and one in which it escapes downstream as a cyclonic warm-core eddy. James (1980) considers the simpler problem of barotropic quasigeostrophic flow over an axisymmetric bump using a finite-difference model and illustrates similar dynamics to those seen in the more complicated model of Huppert and Bryan (1976). When the eddy is partially trapped, a patch of positive vorticity spirals onto the hill, and successive pieces of it break away and then coalesce back into the main patch of positive vorticity. Because of the finite-difference nature of this model, friction is always present. Verron and LeProvost (1985) study the quasigeostrophic model, including the effect of beta. Kozlov (1983) uses the inviscid method of contour dynamics to demonstrate the two dynamical regimes of the quasigeostrophic problem. More recently Chapman and Haidvogel (1992) study the problem of flow over finite topography in a continuously stratified primitive equation model.

To understand flow over tall seamounts in the ocean, one must look beyond traditional quasigeostrophic dynamics, which allow the fractional height of the topography to be only order Rossby number. In addition, stratification must be taken into account since the flow structure in the ocean changes with depth. To incorporate these effects in a simple model, we discuss flow in a two-layer fluid over a right circular cylinder that goes all of the way through the lower layer and only an order Rossby number amount into the upper layer, and compare the solutions to traditional quasigeostrophic solutions where the cylinder height is order Rossby number. The model geometry allows consideration of an obstacle that has both finite vertical and horizontal cross sections, capturing both classes of quasigeostrophic solutions described by Buzzi and Speranza (1979). In section 2, the model geometry is discussed and steady solutions are presented for background flow with and without shear. In section 3, the initial value problem is considered, first by reviewing the work of Kozlov (1983) with the one-layer model and then by extending this work to the two-layer model, considering flow over both small and finite topography.

2. Steady solutions

Two model geometries are considered. The first is representative of traditional quasigeostrophic models (Fig. 1a). The topography is contained completely within the lower layer, and as such is coincident with an isopycnal surface. The second model geometry allows the interface to intersect the topography (Fig. 1b) and therefore allows solutions in a new parameter range.

The formulation of the problem closely follows that of McCartney (1975). The scaling is the same as his except that the upper layer is indexed as 1 and the lower layer as 2. The parameters in this inviscid theory are

$$\epsilon = \frac{U_0}{f_0 L},$$

the Rossby number using the depth-averaged root-mean-square velocity,

$$d = \frac{d'}{H},$$

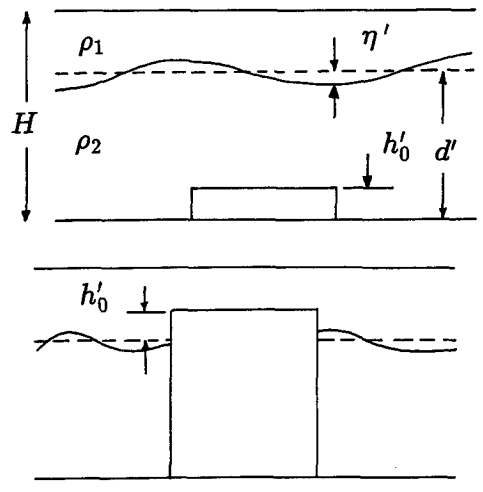

FIG. 1. Side view of the two models. The topography has radius L. (a) Two-layer model with small topography. The lower-layer depth is d' while the density of the upper and lower layers is ρ_1 and ρ_2, respectively. (b) Two-layer model with finite topography. The topography extends an order Rossby number amount into the upper layer and the interface intersects the topography. The relevant topographic perturbation is given by h_0'. The prime quantities are dimensional.

where d' is the depth of the lower layer and H is the total depth,

$$\Gamma^2 = \frac{f_0^2 \rho_0 L^2 d}{g' H \Delta\rho (1-d)},$$

a stratification parameter which is the ratio of the radius of the bump to the deformation radius, and

$$U_0^2 = (1-d)\mathcal{U}_1^2 + d\mathcal{U}_2^2,$$

where $\mathcal{U}_1$ and $\mathcal{U}_2$ are the velocities in the upper and lower layer, respectively. The topographic scale for the small bump model is

$$h_0 = \frac{h_0'}{H} = \frac{h}{H},$$

while for the finite bump it is

$$h_0 = \frac{h_0'}{H} = \frac{h-d'}{H},$$

where h is the height of the topography.

When Γ is small, the stratification is strong and the two layers are relatively uncoupled. When Γ is large, the stratification is weak and the two layers are strongly coupled. Under the quasigeostrophic approximation, Γ is assumed to be order one and the Rossby number is small. In addition, h_0 is of order Rossby number. This last requirement allows the dynamics to be internally consistent so that the layer depth changes only an order Rossby number amount, and the flow remains quasi-horizontal in each layer.

Under the quasigeostrophic approximation, the two-layer model is governed by the two-layer potential vorticity equations. The formulation for the problem on the beta plane can be found in Thompson (1990). The horizontal velocities are scaled by U_0 and the horizontal length is scaled by L, the radius of the topography. The two-layer equations become

$$\partial_t q_n + J(\psi_n, q_n) = 0, \tag{1}$$

where q_n indicates the quasigeostrophic potential vorticity in the nth layer. Away from the topography

$$q_1 = \nabla^2\psi_1 + (\psi_2 - \psi_1)\Gamma^2 d, \tag{2}$$

and

$$q_2 = \nabla^2\psi_2 + (\psi_1 - \psi_2)\Gamma^2(1-d). \tag{3}$$

The deviation of the interface height from its mean depth is given by

$$\eta = \epsilon[\psi_2 - \psi_1](1-d)d\Gamma^2 \tag{4}$$

and is an order Rossby number quantity. The vertical velocity at the interface is given in the two-layer model by

$$w_1 = \frac{d\eta}{dt} = \epsilon(1-d)d\Gamma^2 J(\psi_1, \psi_2 - \psi_1).$$

In steady state, (1) allows a solution such that q_n is a function of ψ_n for $n = 1, 2$. The functional relationship between the potential vorticity and the streamfunction in each layer is determined by upstream conditions. If the velocity is uniform upstream, $\psi_n = -U_n y$. Thus, using (2):

$$q_1 = -\frac{(U_2 - U_1)d\Gamma^2}{U_1}\psi_1, \tag{5}$$

and likewise using (3):

$$q_2 = -\frac{(U_1 - U_2)(1-d)\Gamma^2}{U_2}\psi_2. \tag{6}$$

Thus, we can let $\psi_n = -U_n y + \phi_n$. Away from the topography we can write from (5) and (6):

$$\nabla^2\phi_2 - \frac{U_1(1-d)\Gamma^2}{U_2}\phi_2 = -\phi_1(1-d)\Gamma^2$$

and

$$\nabla^2\phi_1 - \frac{U_2 d\Gamma}{U_1}\phi_\circ = -\phi_2 d\Gamma.$$

For the small topography model, McCartney (1975) finds an equation for ϕ_1 and requires that ϕ_1 and its first three derivatives in r be continuous at $r = 1$, which is equivalent to the velocity being continuous at $r = 1$ in both layers. The governing equation is

$$\nabla^2(\nabla^2 + k_2^2)\phi_1 = h\Gamma^2, \tag{7}$$

where

$$k_2^2 = -\frac{\Gamma^2}{U_1 U_2}.$$

When k_2^2 is negative, we define

$$\kappa_2^2 = -k_2^2.$$

The fundamental length scale of the problem is set by k_2.

For $r > 1$, (7) applies for the finite bump geometry as well. However, over the topography the potential vorticity is given by

$$q_1 = \nabla^2\psi_1 + \frac{h-d}{\epsilon(1-d)}.$$

The same functional relationship should hold between q_1 and ψ_1 as in (5). Thus, for $r < 1$ over the topography:

$$\psi_1 = \phi_1$$

so that

$$\nabla^2\phi_1 + \phi_1 k_3^2 = -\frac{h_0 - d}{\epsilon(1-d)}, \tag{8}$$

where

$$k_3^2 = \frac{(U_1 - U_2)d\Gamma^2}{U_1}. \tag{9}$$

The sign of k_3^2 depends on the direction and magnitude of the flow in each layer, allowing either a wavelike or an evanescent response. The boundary conditions for the finite depth topography are chosen as follows: the velocity should be continuous in the upper layer, and the velocity normal to the cylinder should vanish in the lower layer (ψ_2 = const at $r = 1$). There is an undetermined constant that is chosen by setting the circulation in the lower layer at zero. This choice is made because it corresponds to the steady-state solution of an initial value problem where the velocity is brought to the final value from rest. If initially there is no circulation and the fluid remains inviscid throughout its evolution, then no circulation develops.

The solutions for ϕ_1 and ϕ_2 can be separated into an island component (odd in y) and a topographic component (even in y). For the problem that McCartney (1975) studied, ϕ_1 and ϕ_2 are purely even and on the f plane are independent of θ, the azimuthal coordinate. For the finite depth model, the odd component is forced by the boundary conditions in the lower layer, while the even component is forced by the topographic contribution to the potential vorticity anomaly. With this simple geometry we capture elements of the two cases that Buzzi and Speranza (1979) discussed.

a. *Barotropic flow*

When the background flow is barotropic ($U_1 = U_2$), $\kappa_2 = \Gamma$. An example of the small bump solutions is shown as a reference for the finite depth results (Fig. 2). The interface is raised uniformly over the topography as a radially symmetric perturbation. The vertical velocity is upstream–downstream symmetric; positive upstream where fluid parcels rise to go over the topography and negative downstream.

For the finite bump geometry for $r > 1$ we have

$$\psi_1 = a_1 \ln r + a_2 K_0(\Gamma r) + a_3 \sin\theta / r + a_4 K_1(\Gamma r) \sin\theta - r \sin\theta, \quad (10)$$

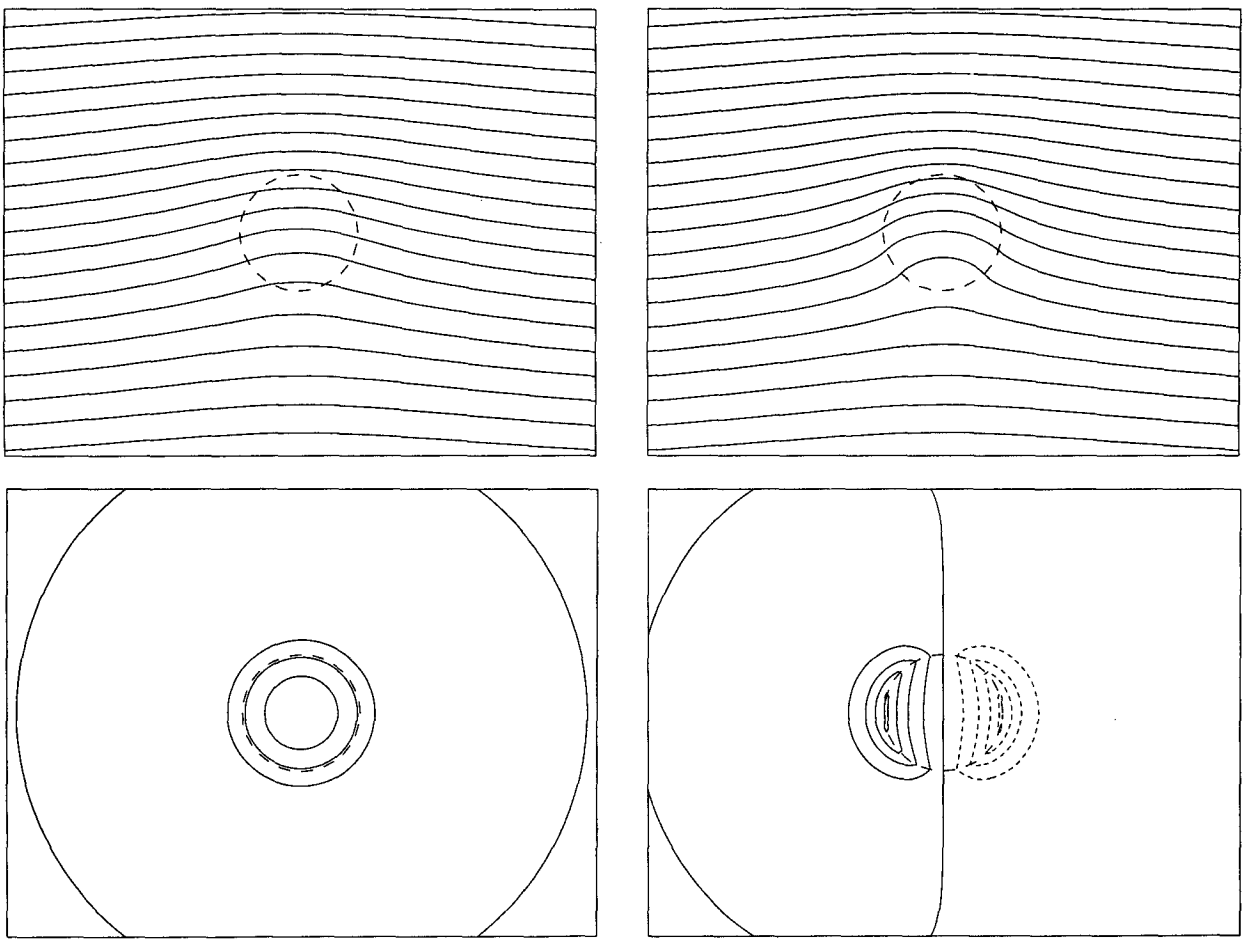

FIG. 2. Solution for flow over small topography with no upstream vertical shear when $h_0 = 1$, $\Gamma = 2$, and $d = 0.5$ ($\delta = 1$). (a) Upper-layer streamlines, (b) lower-layer streamlines, (c) interface height, (d) vertical velocity. In this and all subsequent streamline pictures, the contour interval is 0.4 for the streamlines and 0.1 for the interface height and vertical velocity. The flow is from the left to the right.

and for $r < 1$:

$$\psi_1 = b_1 - \frac{h_0 - d}{4\epsilon(1-d)} r^2 + b_2 r \sin\theta, \quad (11)$$

while

$$\psi_2 = a_1 \ln r - \delta a_2 K_0(\Gamma r) + a_3 \sin\theta / r - \delta a_4 K_1(\Gamma r) \sin\theta - r \sin\theta, \quad (12)$$

where $\delta = H_1/H_2 = (1-d)/d$. Applying the matching conditions we find that

$$a_1 = -\frac{q_a}{2},$$

$$a_2 = \frac{q_a K_0(\Gamma)}{2K_1(\Gamma) + K_0(\Gamma)},$$

$$a_3 = \frac{2K_1(\Gamma) + K_0(\Gamma)}{2(1+\delta)K_1(\Gamma) + K_0(\Gamma)},$$

$$b_1 = q_a\left(\frac{K_0(\Gamma)}{2\Gamma K_1(\Gamma)} + \frac{1}{4}\right),$$

and

$$b_2 = \frac{2(1+\delta)K_1(\Gamma)}{2(1+\delta)K_1(\Gamma) + K_0(\Gamma)}.$$

We have defined

$$q_a = \frac{h_0(1+\delta)}{\epsilon\delta}, \quad (13)$$

which is the magnitude of the potential vorticity anomaly in the upper layer. The potential vorticity anomaly is defined by the right-hand side of (8) and is the stretching vorticity induced when fluid parcels cross the topography. Notice that a_3 and b_2 are independent of q_a and give the amplitude of the even or axisymmetric component of the flow, while a_1, a_2, and b_1 give the amplitude of the odd (dependent on θ) component and are independent of q_a. From the form of the solution, one can tell that the axisymmetric flow (bumplike, Buzzi and Speranza 1979, their case 1) falls off as r^{-1} while the θ-dependent component (islandlike, Buzzi and Speranza 1979, their case 2) falls off as r^{-2} in the far field.

An example of the finite depth solution is shown in Fig. 3. The odd component results in an interface which is asymmetric and is higher in the north than in the south, while the fluid is split by the topography in the lower layer. The asymmetric response of the interface is in accord with results from primitive equation models (Chapman and Haidvogel 1992). The interface near the topography in the south is depressed, responding to the anticyclonic perturbation in the upper layer and the requirement of no circulation in the lower layer. The vertical velocity also exhibits the left–right asymmetry. If $q_a = 0$ then the interface would be tilted symmetrically north–south, since all of the radially symmetric terms in the solution would vanish.

To understand the general structure of the solution, we can calculate various critical topographic heights. Ou (1991) has calculated these critical heights also. The critical topographic height above which closed streamlines form in the lower layer for the small topography model is

$$\frac{h_{s2}}{\epsilon} = \frac{d}{\frac{1}{2}d + (1-d)I_1(\Gamma)K_1(\Gamma)},$$

while the critical height for the upper-layer streamlines to close, h_{s1}, is found numerically. For reference, the critical height for closed streamlines to form in a one-layer model is $2\epsilon D$ where D is the layer depth. Thus in the weak stratification limit, the model behaves barotropically and $h_{s1} = h_{s2} = 2\epsilon$. On the other hand, in the strong stratification limit, $h_{s1} \to \infty$ because it becomes uncoupled from the dynamically active lower layer, while $h_{s2} = 2\epsilon d$, the one-layer limit. These predictions are born out in Fig. 4a.

From the solution (10), (11), and (12), the critical height for closed streamlines to occur in the upper layer in the finite depth model is

$$\frac{h_{\text{crit}}}{\epsilon} = \frac{4(1-d)}{2 + d\Gamma K_0(\Gamma)K_1(\Gamma)}. \quad (14)$$

In the strong stratification limit $h_{\text{crit}} \to 2\epsilon(1-d)$, the one-layer result for a layer with depth of the upper layer; when the stratification is weak, the critical height approaches zero (Fig. 4a).

Both h_{crit} and h_{s2} are monotonic function of d, with h_{crit} having the opposite tendency of h_{s2}. The limiting cases can be predicted from the one-layer results. When $d \to 1$, h_{s2} has a maximum value of 2ϵ; when $d \to 0$, h_{s2} approaches zero. In interpreting these results, it is important to point out that if d changes by an order one amount in the finite depth model, the total topographic height changes by an order one amount; however, in the small bump model, this is not the case.

The solutions of the finite depth model must be tested to see if they are physically reasonable. If the interface goes above the topography anywhere, the model geometry is no longer consistent. The critical height for this to occur is found from $\eta = h_0$ in (4). It is given by

$$\frac{h\eta}{\epsilon} = \frac{4\Gamma^2 K_1(\Gamma)^2 \delta\Gamma}{(2\sqrt{\delta}K_1(\Gamma) + K_0(\Gamma)) \times (2K_1(\Gamma)(1+\delta) + K_0(\Gamma)\Gamma)}. \quad (15)$$

The maximum interface height always occurs at $\theta = \pi/2$ and $r = 1$ for eastward flow on the f plane. For a physically consistent solution h_0 must be greater than h_η. The critical height is a monotonically increasing function of stratification, and in general is larger for

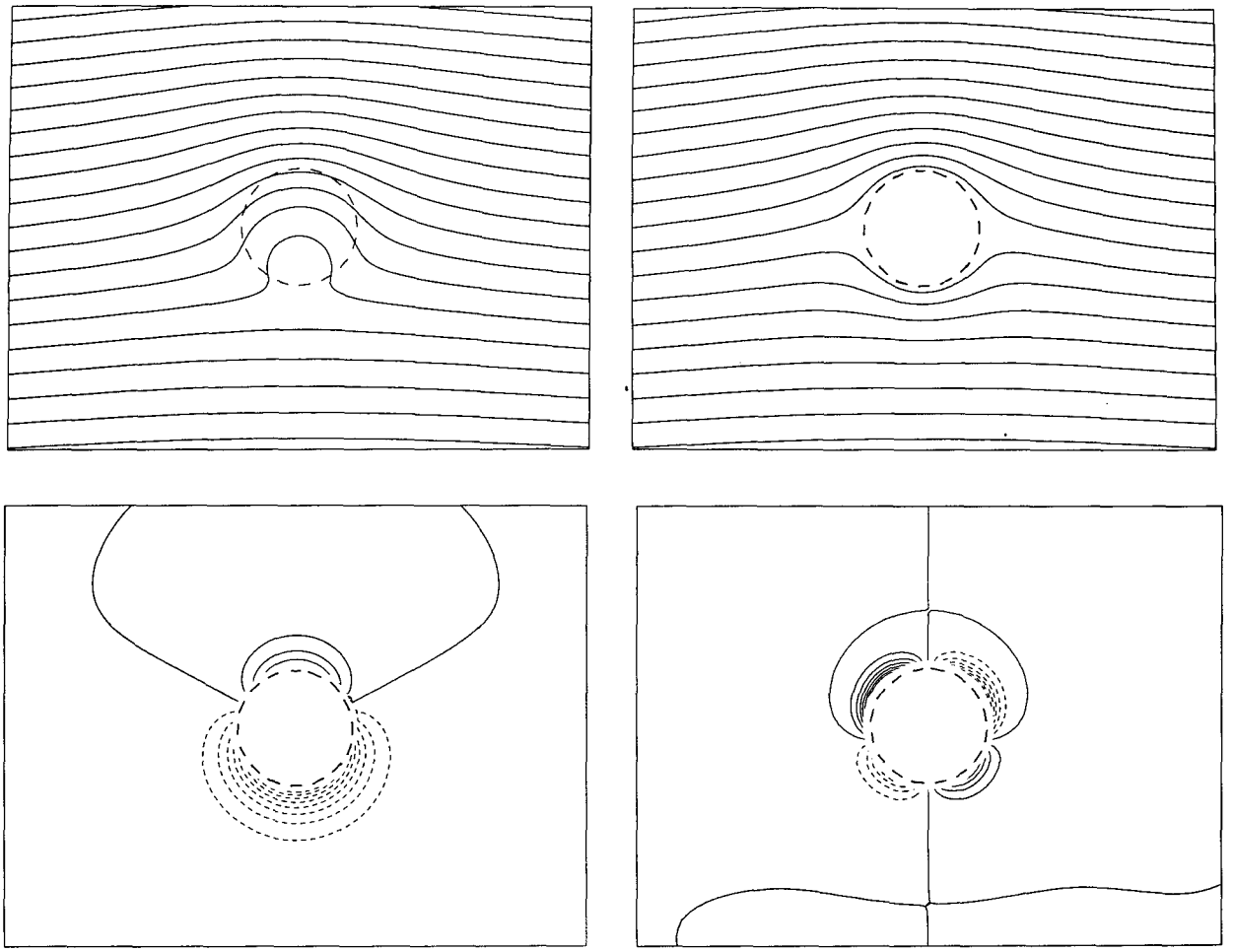

FIG. 3. Solution for flow over finite topography with no upstream vertical shear using the same parameters as in Fig. 2. (a) Upper-layer streamlines, (b) lower-layer streamlines, (c) interface height, and (d) vertical velocity.

smaller values of d (Fig. 4b). When the stratification is large (Γ small), h_η approaches zero, implying that h_0 could be quite small and the solution would still be valid. In this limit the interface is stiff and its vertical deflection is limited. When the stratification is weak (Γ large), the fluid responds barotropically and h_η/ϵ approaches $4\delta/(1 + 2\sqrt{\delta})$.

b. *Flow on the f plane with vertical shear*

Because of the simplicity of the model geometry the interaction between the effects of vertical shear and finite topography can be examined. In this case $k_3^2 = (U_1 - U_2)\Gamma^2 d/U_1$ indicating a wavelike solution when $U_1 > U_2$. For $r > 1$ we have

$$\psi_1 = a_1 \ln r + a_2 K_0(\kappa_2 r) + a_3 \frac{\sin\theta}{r} + a_4 K_1(\kappa_2 r)\sin\theta - r\sin\theta$$

and

$$\psi_2 = a_1 \ln r - \delta a_2 K_0(\kappa_2 r) + a_3 \frac{\sin\theta}{r} - \delta a_4 K_1(\kappa_2 r)\sin\theta - r\sin\theta.$$

For $r < 1$

$$\psi_1 = \frac{h_0 - d}{\epsilon(1 - d)k_3^2} + b_1 J_0(k_3 r) + b_2 J_1(k_3 r)\sin\theta.$$

The stationary waves over the topography come from the effective potential vorticity gradient across streamlines. The background vertical shear maintains the potential vorticity gradient in the exterior. The response in the exterior does not support stationary waves; it is trapped to the topography as evanescent waves. Because of the wavelike character over the topography, the flow is possibly barotropically unstable (e.g., Lorenz 1972).

In the limit of the largest vertical shear allowed in the model, no flow in the lower layer, the solution gives

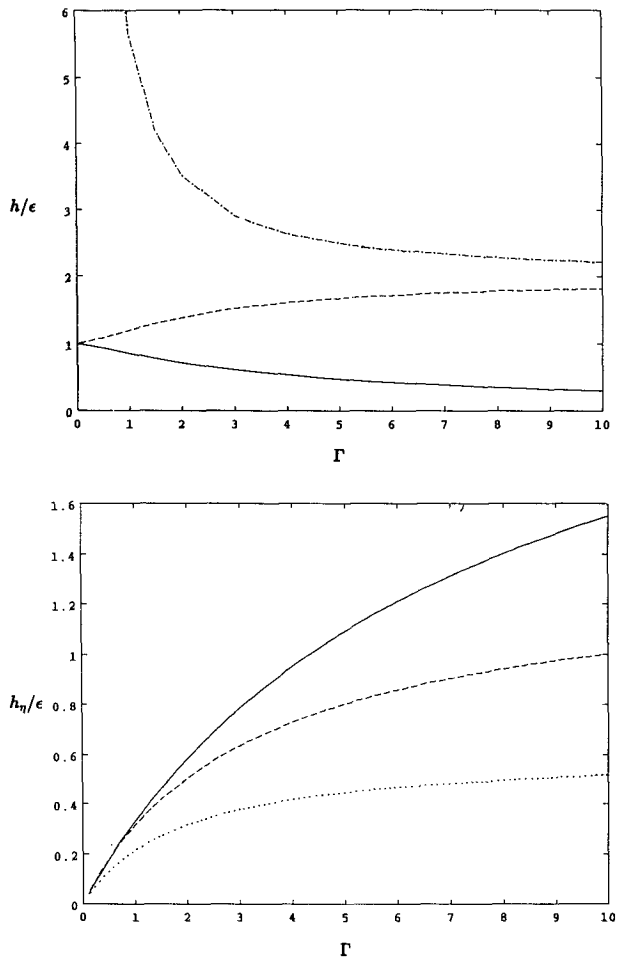

FIG. 4. Critical heights of the two-layer models. (a) Critical height when $\delta = 1$ for both the finite depth topography model and the small topography model. The solid line is h_{crit}/ϵ, the critical height for closed streamlines to form in the finite depth model. The dashed line is h_{s2}/ϵ, the critical height for closed streamlines to form in the small topography model in the lower layer. The dotted–dashed line is h_{s1}/ϵ, the critical height for closed streamlines to form in the upper layer of the small topography model. (b) Critical height h_η/ϵ as a function of Γ, for $d = 0.25$ (solid line), $d = 0.5$ (dashed line), and $d = 0.75$ (dotted line).

$\psi_2 = 0$ everywhere. In this case, $k_3^2 = \Gamma^2 d$ and $U_1 = \sqrt{1/(1-d)}$. The exterior solution is written

$$\psi_1 = a_1 \ln r + a_3 \sin\theta/r - U_1 r \sin\theta. \quad (16)$$

The coefficients are found by matching across $r = 1$ and are given by

$$a_1 = -\frac{J_1(k_3)q_a}{k_3 J_0(k_3)},$$

$$a_3 = U_1 \frac{k_3 J_0(k_3) - 2J_1(k_3)}{k_3 J_0(k_3)},$$

$$b_1 = \frac{q_a}{k_3^2 J_0(k_3)},$$

and

$$b_3 = -\frac{2U_2}{k_3 J_0(k_3)}.$$

The height of the topography at which closed streamlines appear is given by

$$\frac{h_{crit}}{\epsilon} = \frac{2(1-d)U_1}{J_1(k_3)[k_3 J_0(k_3) - J_1(k_3)]}. \quad (17)$$

At zeros of J_1 the critical height becomes infinite. At this point, a resonant solution is present, similar to the one described by McCartney (1975) for eastward flow on the β-plane. The resonant solution may be an artifact of the shape of the topography, although the wavelike character is not.

The maximum value of η is

$$\frac{\eta_{max}}{\epsilon} = \left| \frac{2U_1 \Gamma^2 d(1-d)J_1(k_3)}{k_3 J_0(k_3)} \right|, \quad (18)$$

independent of the topographic height h_0, depending on the background shear and stratification. Once again the resonance is present; when k_3 is a zero of J_1 then η_{max} goes to zero. When k_3 is a zero of J_0, η_{max} becomes infinite. In general, the interface is more likely to go over the topography when the shear is strong, which increases the left–right tilt of the interface. An example of the solution is shown in Fig. 5 which shows the tilt of the interface.

3. Time-dependent solutions

The initial value problem of flow impinging on topography is explored next. If only barotropic incoming flow on the f plane is considered, the method of contour dynamics can be used. We consider barotropic incoming flow on the f plane and use the method of contour dynamics, extending the work of Kozlov (1983) by adding a second layer. To solve for the flow in the finite depth case, the method must be modified so that the matching and boundary conditions at the boundary of the topography can be handled.

a. Flow in one layer over small topography

The evolution of the one-layer fluid is determined by the quasigeostrophic potential vorticity equation of the same form as (1) where the nondimensionalized potential vorticity is given by

$$q = \nabla^2 \psi + \frac{h}{\epsilon}.$$

If the vorticity, the topography, and the boundary conditions are known we can calculate the streamfunction using a Green's function:

$$\psi(x, y) = \iint q(x', y') G(x, x', y, y') dx' dy' + \text{boundary contributions.} \quad (19)$$

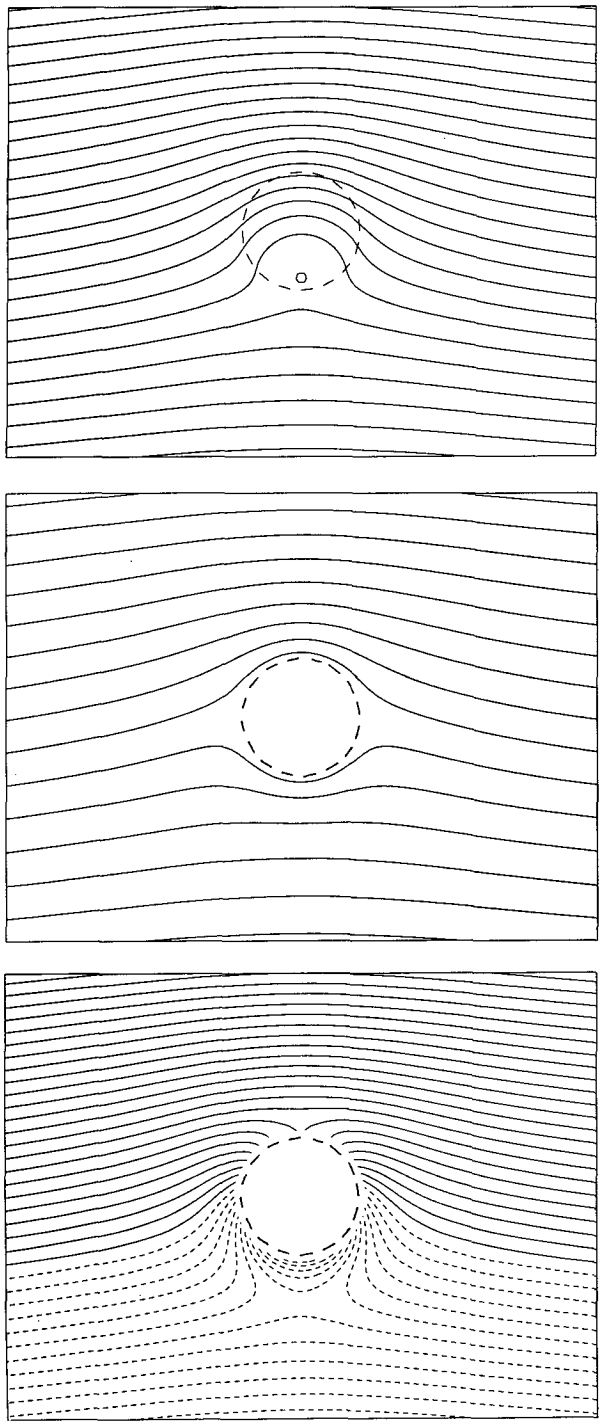

FIG. 5. Solution for flow over finite topography with upstream vertical shear, $U_1 = 1.2$, when $h_0 = 1$, $\Gamma = 2$ and $d = 0.5$. (a) Upper-layer streamlines, (b) lower-layer streamlines, and (c) interface height.

For Laplace's equation in an infinite domain, the Green's function takes the simple form:

$$G(x, x', y, y') = \frac{1}{2\pi} \ln R, \qquad (20)$$

where $R = [(x - x')^2 + (y - y')^2)]^{1/2}$. If the potential vorticity q is piecewise constant, it can be taken out of the integral. In order to calculate the velocity at any point, (19) is differentiated with respect to x and y, the symmetry of the Green's function is invoked, and Green's theorem is used to obtain

$$(u, v) = (-\partial_y \psi, \partial_x \psi) = q \oint_{\partial D} G(R)(dx', dy'). \qquad (21)$$

The velocity at any point is found by doing the contour integral.

The method reduces the problem of solving for the nonlinear evolution of the field to that of evaluating (21) at each time step. Once the velocity on ∂D is known, then it can be stepped forward in time to find the new location of the contour. The implementation of the technique used is described in Polvani (1988). At each time step, the boundary of the region of constant relative vorticity is stepped forward via Runge–Kutta integration. The Green's function is singular on the contour, but the singularity can be handled as in Polvani's (1988) appendix B. The contour dynamics computer code used here was developed by Meacham (1991). As the contour deforms with time, the distances between the points on the contour change, and an adjustment in the spacing of the points on the contour must be made to accurately carry the calculation forward in time. The points are redistributed according to the local rate of curvature. In addition, points are added or removed as needed, and when the contour comes back on itself, it is pinched off. Only when many (on the order of 10) pinch-offs have occurred is there a significant (on the order of several percent) loss of vorticity.

After the flow has been turned on, there are two different regions of nonzero vorticity (Fig. 6). The region of fluid that originated upstream and moves over

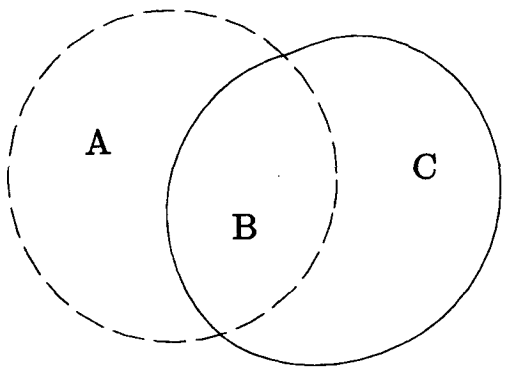

FIG. 6. Schematic of the different regions of constant relative vorticity. Outside of the two contours, the vorticity is zero. In region A the vorticity is anticyclonic with value $-h_0/\epsilon$. In region B the vorticity is zero. In region C the vorticity is cyclonic with value h_0/ϵ. The circular dashed contour delineates the boundary of the topography. The solid contour delineates the boundary of the fluid which originated over the topography.

the topography (region A) has relative vorticity $-h_0/\epsilon$; the region of fluid that originated over the topography and moves off the topography (region C) has relative vorticity h_0/ϵ. Region B has no relative vorticity and is composed of fluid parcels that originated over the topography and remain there. Instead of evaluating the contours that bound regions A and C separately, we evaluate the topographic contour (a circle) using potential vorticity $-h_0/\epsilon$ and the contour that bounds the fluid that originated over the topography using potential vorticity h_0/ϵ and add the results to take advantage of the cancellation in region B. This method can be used for any arbitrarily shaped region and is not restricted to a circle. Like Kozlov (1983), we consider flow over a circular cylinder where the contour integral around the circular topography can be done analytically.

For reference, we repeat Kozlov's (1983) calculation to show the two dynamical regimes, complete shedding, and partial shedding of the fluid that originated over the topography (Fig. 7). When the background flow is strong, all of the fluid is shed downstream, and the

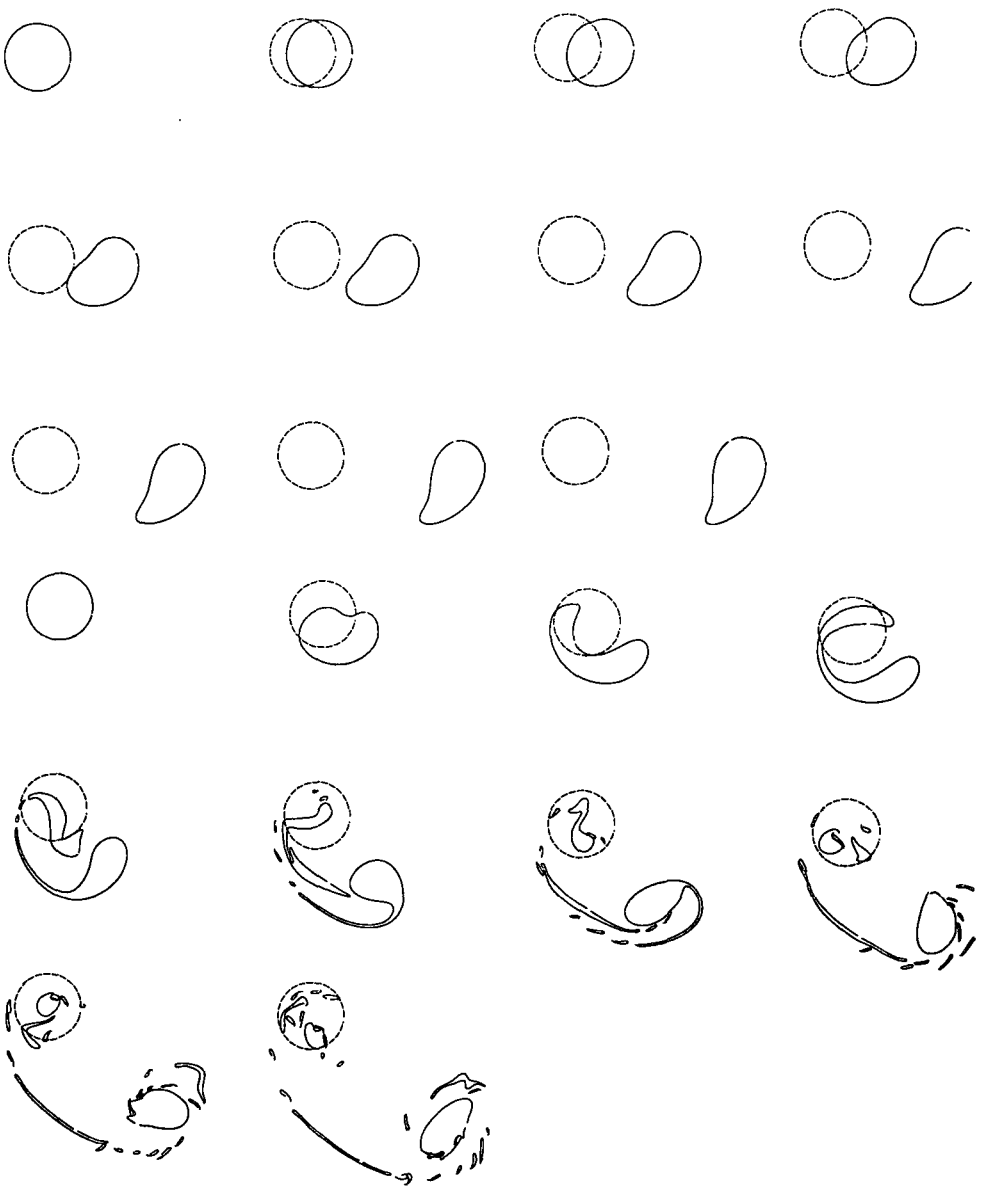

FIG. 7. Time evolution of the contour for a case when all of the fluid is shed downstream. (a) $h_0/\epsilon = 1$ and the flow is turned on abruptly at $t = 0$. Times are $t = 0, 1, \cdots, 10$ with time increasing to the right and downward. The dashed contour is the boundary of the topography; the solid contour delineates the boundary of the fluid that originated over the topography, and (b) $h_0/\epsilon = 5$ at $t = 0, 1, \cdots, 9$.

contour changes from a circle to a tear-drop shape as it is influenced by the cyclonic circulation over the topography, but it remains coherent. The shed fluid remains close to the x axis as it moves downstream. When the background flow is weak, some of the fluid remains trapped over the topography, while some is shed downstream.

b. Flow in two layers over small topography

In this section, the work of Kozlov is extended to include a second layer; we begin by studying the small topography model. This work is similar to that done by Davey et al. (1992) who also studied this problem with the contour dynamics model. Here we stress a comparison between the results from the small topography model and the finite topography model. The additional dynamics are illustrated by considering two situations: one in which the stratification is strong and the other in which the stratification is weak. We choose the topographic height so that comparisons can be made to the one-layer examples discussed in section 3a. As is apparent from the steady solutions, there are two additional free parameters in this problem: δ, the relative height of the two-layer depths, and Γ, the inverse of the Rossby radius of deformation.

The time-dependent dynamics are governed by (1) where

$$q_1 = \nabla^2\psi_1 + \frac{(\psi_2 - \psi_1)\Gamma^2}{1+\delta},$$

and

$$q_2 = \nabla^2\psi_2 + \frac{(\psi_1 - \psi_2)\Gamma^2\delta}{1+\delta} + \frac{h(1+\delta)}{\epsilon}.$$

The contour over the topography can be done analytically to take advantage of the cancellation over the topography giving

$$\psi_1' = \begin{cases} \dfrac{h_0}{\epsilon}\left(\dfrac{K_1(\Gamma)}{\Gamma} I_0(\Gamma r) - \dfrac{1}{4} r^2\right), & r < 1 \\ \dfrac{h_0}{\epsilon}\left(-\dfrac{I_1(\Gamma)}{\Gamma} K_0(\Gamma r) - \ln r\right), & r > 1, \end{cases}$$

and

$$\psi_2' = \begin{cases} \dfrac{h_0}{\epsilon}\left(-\delta\dfrac{K_1(\Gamma)}{\Gamma} I_0(\Gamma r) - \dfrac{1}{4} r^2\right), & r < 1 \\ \dfrac{h_0}{\epsilon}\left(\delta\dfrac{I_1(\Gamma)}{\Gamma} K_0(\Gamma r) - \ln r\right), & r > 1. \end{cases}$$

This is McCartney's (1975) steady solution for flow over small topography excluding the background flow. The contribution from the contour integral is

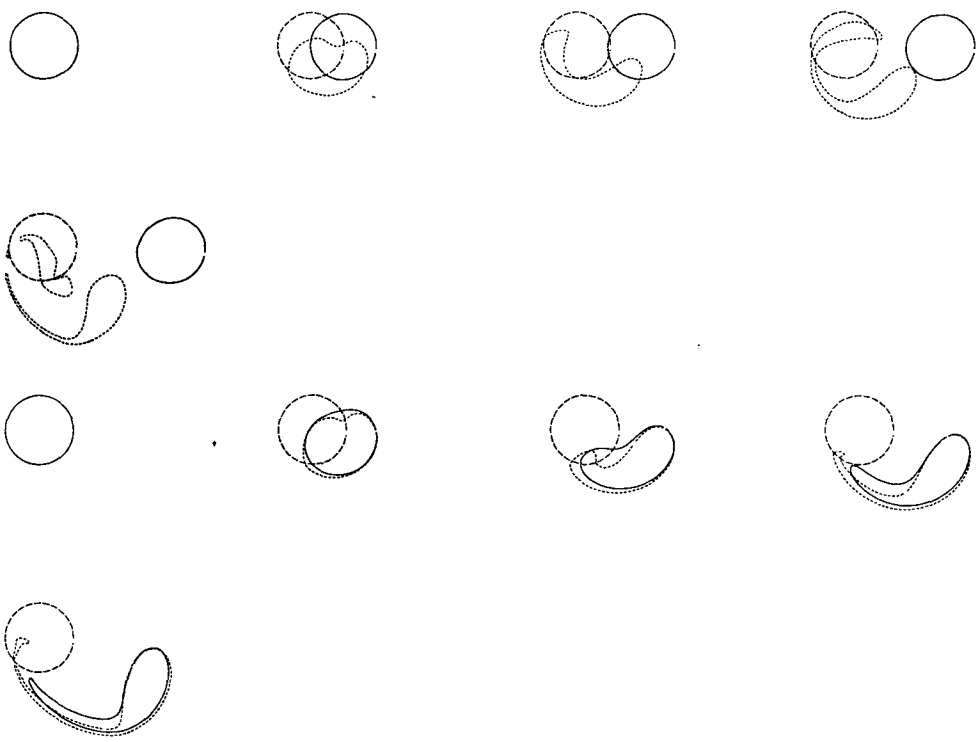

FIG. 8. Time evolution of the contours delineating fluid that originated over the topography in the upper layer (solid) and in the lower layer (dashed) in the two-layer small topography model for (a) $\Gamma = 0.25$, $\delta = 1$, and $h_0/\epsilon = 2.5$ at $t = 0, 1, 2, 3, 4$ and (b) $\Gamma = 4$.

$$\psi_i(x, y) = \frac{1}{2\pi} \iint \frac{h_0(1+\delta)}{\epsilon\delta} G_{ij}(R) dx'dy', \quad (22)$$

where $R = [(x - x')^2 + (y - y')^2]^{1/2}$ and G_{ij} is the Green's function that represents the effect on a point in layer i of a point vortex in layer j (Polvani 1988). For this problem, a subset of the G_{ij} is needed since the vorticity is zero everywhere except within the region of fluid that originated over the topography in the lower layer. These Green's functions are given by

$$G_{12} = \frac{1}{1+\delta} \ln R + \frac{1}{1+\delta} K_0(\Gamma R) \quad (23)$$

and

$$G_{22} = \frac{1}{1+\delta} \ln R - \frac{\delta}{1+\delta} K_0(\Gamma R), \quad (24)$$

where K_0 is the modified Bessel function of order zero.

Since the upper-layer potential vorticity is always zero, the interface height can be calculated by finding the relative vorticity in the upper layer:

$$\eta = \frac{\Gamma^2\delta(\psi_2 - \psi_1)}{(1+\delta)^2} = -\frac{\delta\nabla^2\psi_1}{1+\delta} \quad (25)$$

from (3). The relative vorticity can be calculated directly from the contour integral (22):

$$\nabla^2\psi_2 = v_x - u_y$$

$$= \oint_{\partial D} \frac{G'_{21}(R)}{R} [(x - x')dy' - (y - y')dx']. \quad (26)$$

There is no singularity in this integral, which is done in the upper layer since the singularities in the Green's function are in the lower layer. In each run, a contour delineating the fluid that originates over the topography in the upper layer is followed throughout the evolution of the flow. This contour is dynamically inactive but marks the movement of the particles that originated over the topography in the upper layer.

With strong stratification the upper-layer contour is not coincident with the lower-layer contour, and the response is baroclinic (Fig. 8a). The lower layer responds nearly as a one-layer fluid as described in section 3a, and the lower-layer contour evolution in Fig. 8a is very similar to the contour in Fig. 7b. The upper-layer contour moves off downstream with little distortion.

With weak stratification, the fluid responds nearly barotropically (Fig. 8b). This is shown by the near coincidence of the contours in the upper and lower layers. Less fluid remains over the topography when the stratification decreases because the disturbance is less bottom trapped, as predicted by the higher value for the critical height h_{s2} calculated in section 2b. For this example, we proceed to calculate the flow in both layers (Fig. 9). The flow field is slightly bottom intensified both near the bump and in the shed eddy. The interface is raised over the topography, and the shed eddy carries a warm anomaly downstream (Figs. 10 and 11) as demonstrated in the primitive equation model of Huppert and Bryan (1976). When the topographic height is the same as the example shown in Fig. 7b, the development of the lower-layer contour is similar to the one-layer example (Fig. 12). This results because when the stratification is weak, the perturbation is weakly bottom trapped. However, the baroclinic nature of the flow is revealed since the contours in the two layers are not entirely coincident.

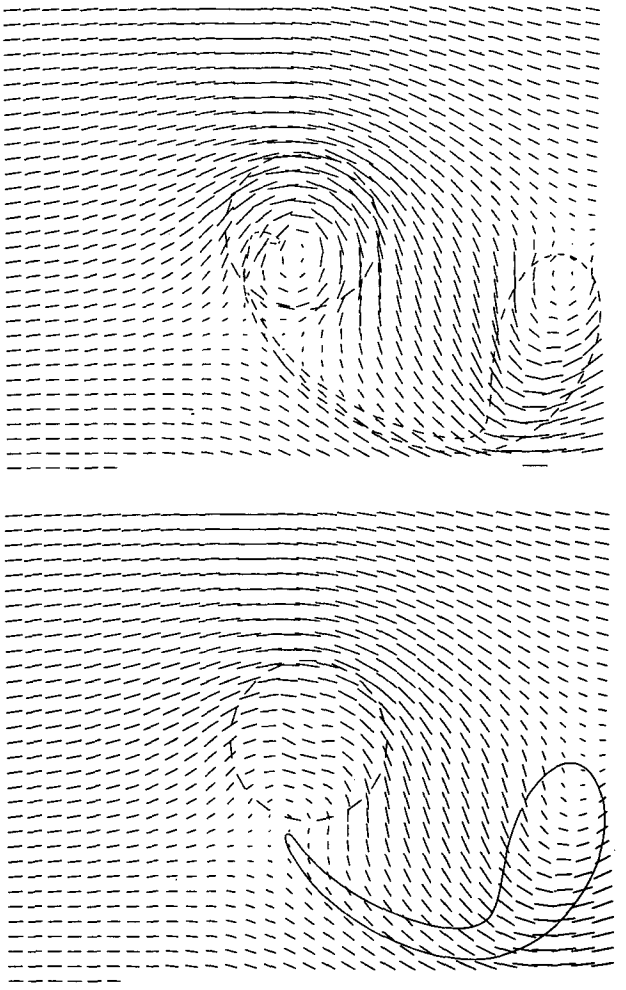

FIG. 9. Flow field of the fluid for the case shown in Fig. 8b at $t = 4$: (a) lower layer, (b) upper layer.

c. *Flow over finite topography in two layers*

For the finite depth model, the method of solution is different than that used in sections 3a and 3b because of the boundary and matching conditions that must be applied at the edge of the topography. The problem is therefore solved in two regions and then a zero potential vorticity solution is used to match the two regions together.

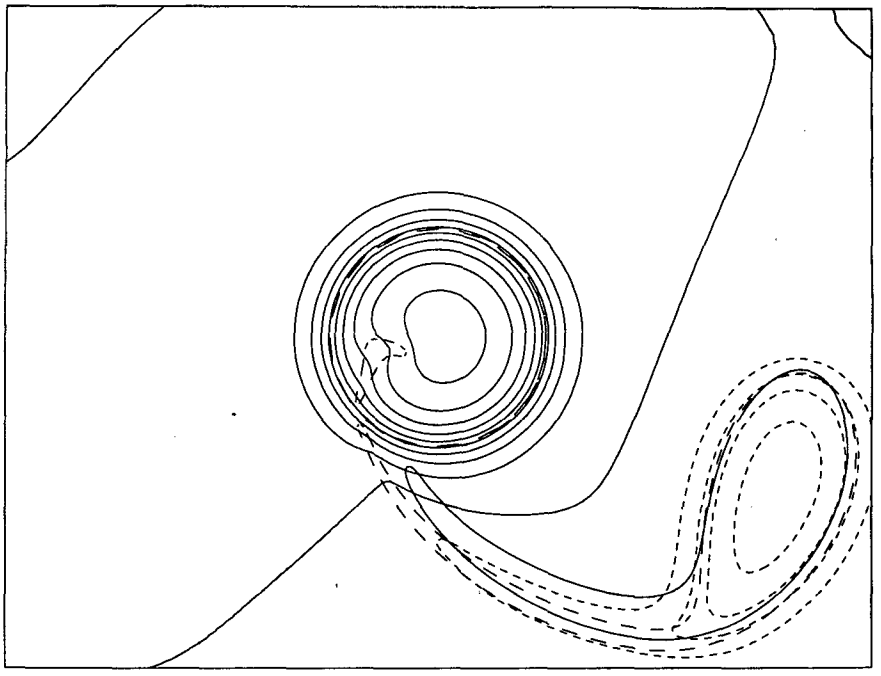

FIG. 10. Interface displacement for the case shown in Fig. 8b at $t = 4$. Dashed contours indicate negative interface displacement. The interface is high over the topography and low over the shed eddy. The solid line outside of $r = 1$ is the contour which delineates fluid that originated over the topography in the upper layer; the line with the longer dashes delineates the fluid that originated over the topography in the lower layer.

In the inner region ($r < 1$), the one-layer logarithmic Green's function (20) applies. In the outer region ($r > 1$), the Green's functions are similar to those used in (23) and (24), but this time the singularity is located in the upper layer. The Green's functions needed in the outer region are

$$G_{11} = \frac{\delta}{1+\delta}\ln R - \frac{1}{1+\delta}K_0(\Gamma R) \qquad (27)$$

and

$$G_{12} = \frac{\delta}{1+\delta}\ln R - \frac{\delta}{1+\delta}K_0(\Gamma R). \qquad (28)$$

In order to find the zero potential vorticity or homogeneous solution, the contribution to the velocity from the contour integral is found at $r = 1+$ for the upper and lower layers by doing the contour integral around region C in Fig. 6 and for the upper layer at $r = 1-$ by doing the contour integral around region A in Fig. 6. This velocity is then transformed into cylindrical coordinates, and application of a fast Fourier transform decomposes the velocity into a sum of modes in θ. Thus at $r = 1+$, the contribution to the velocity from the contour integral can be written as

$$u_c^{(j)}\ (\theta, r = 1+) = \sum_{n=-N/2}^{N/2} u_n^{(j+)} e^{-in\theta} \qquad (29)$$

$$v_c^{(j)}\ (\theta, r = 1+) = \sum_{n=-N/2}^{N/2} v_n^{(j+)} e^{-in\theta}, \qquad (30)$$

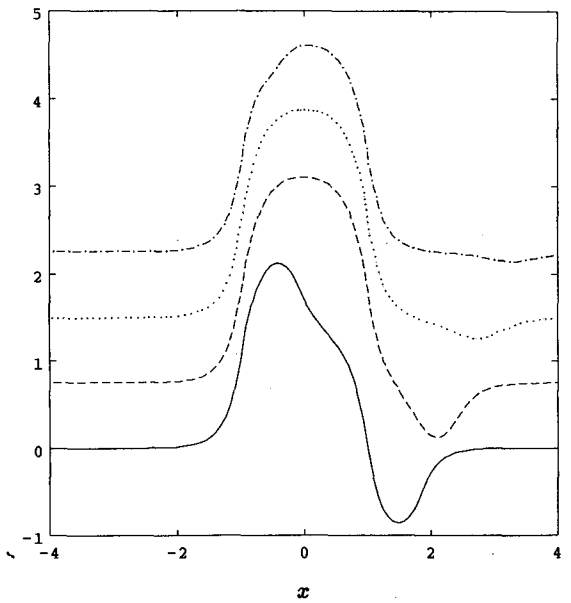

FIG. 11. Interface displacement for the case shown in Fig. 8b for a cut along the x axis at $t = 1, 2, 3, 4$. Notice that the cut is not taken through the center of the eddy, so that the maximum interface displacement is larger than shown. The interface is offset by 0.75 for $t = 2$, 1.5 for $t = 3$, and 2.25 for $t = 4$.

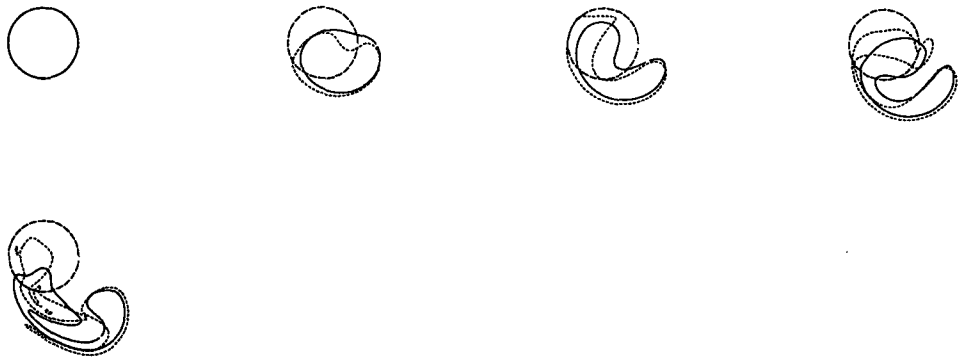

FIG. 12. Time evolution of the contours delineating fluid that originated over the topography in the upper layer (solid) and in the lower layer (dashed) in the two-layer small topography model, $\Gamma = 4$, $\delta = 1$, and $h_0/\epsilon = 5$; $t = 0, 1, 2, 3, 4$.

where $j = 1, 2$ and

$$u_c^{(1)} \quad (\theta, r = 1-) = \sum_{n=-N/2}^{N/2} u_n^{(1-)} e^{-in\theta} \qquad (31)$$

$$v_c^{(1)} \quad (\theta, r = 1-) = \sum_{n=-N/2}^{N/2} v_n^{(1-)} e^{-in\theta} \qquad (32)$$

for the velocity in the inner region (where now u is the radial velocity and v is the azimuthal velocity).

The homogeneous solutions for the streamfunctions are written:

$$\psi^{(1h)} = \sum_{n=-N/2}^{N/2} a_n K_{|n|}(\Gamma r) e^{-in\theta} + b_n r^{-|n|} e^{in\theta} + b \ln r \qquad (33)$$

and

$$\psi^{(2h)} = \sum_{n=-N/2}^{N/2} -\delta a_n K_{|n|}(\Gamma r) e^{-in\theta} + \mathrm{b}_n r^{-|n|} e^{in\theta} + b \ln r \qquad (34)$$

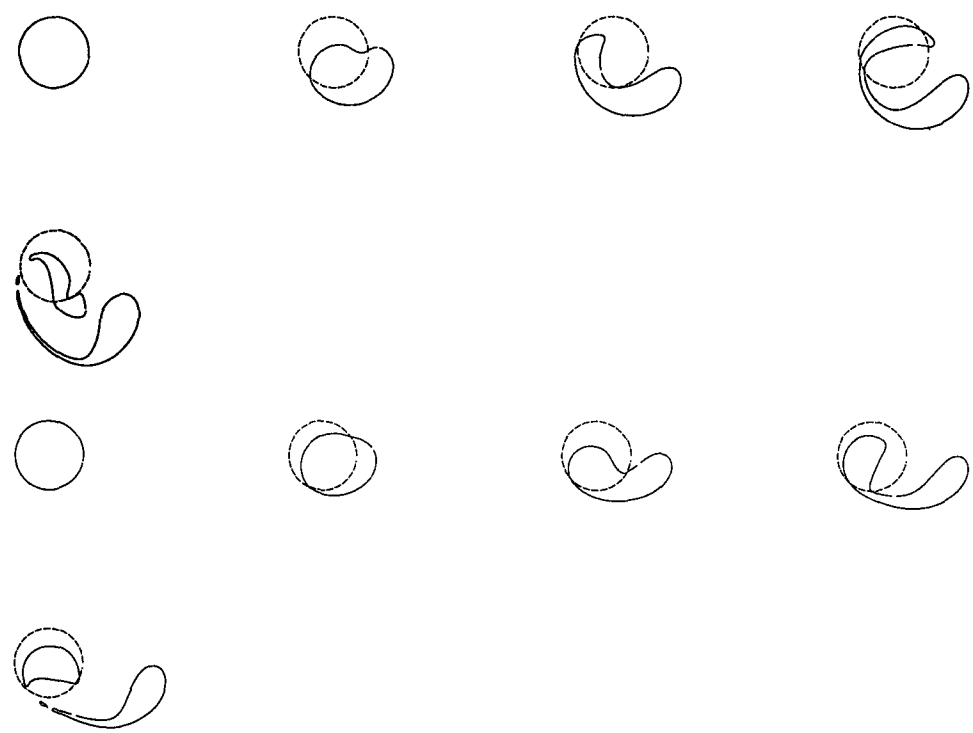

FIG. 13. Time evolution of the contour that delineates fluid that originated over the topography in the upper layer in the two-layer finite topography model for (a) $\Gamma = 0.25$, $\delta = 1$, and $h_0/\epsilon = 2.5$ at $t = 0, 1, 2, 3, 4$ and (b) $\Gamma = 4$.

for $r > 1$ and

$$\psi^{(1h)} = \sum_{n=-N/2}^{N/2} c_n r^{|n|} e^{in\theta} \tag{35}$$

for $r < 1$.

The boundary conditions at the topography in the lower layer are satisfied independently for each mode. For no flow normal to the boundary in the lower layer we have

$$in(a_n \delta b_n K_n) + u_n^{(2+)} = 0. \tag{36}$$

The condition on the circulation reduces to

$$-\delta \Gamma K_0'(\Gamma) + b + v_0^{(2+)} = 0. \tag{37}$$

The velocity in both directions must match in the upper layer. These conditions are satisfied when

$$u_n^{(1-)} + inc_n = in(a_n + b_n K_n(\Gamma)) + u_n^{(1+)} \tag{38}$$

and

$$v_n^{(1-)} + nc_n = -na_n + \Gamma b_n K_n'(\Gamma) + b\delta_{n0} + v_n^{(1+)}, \tag{39}$$

where δ_{ij} is the Kronecker delta. We note that for a real solution $a_n = a^*_{-n}$ and $b_n = b^*_{-n}$. For $n = 0$, there is no contribution from the contour integral so that $u_0^{(1-)} = u_0^{(1+)} = 0$ because the radial velocity is given by $u = -\psi_\theta / r$ and the lowest order mode in θ of this is zero. The coefficients in (33), (34), and (35) are solved for using (36), (37), (38), and (39). The contributions to the velocity are determined by analytically differentiating (33), (34), and (35). In practice, 16 modes in θ were sufficient. The check on the method was to keep track of the total vorticity in the system and make sure that it was conserved.

After each numerical run, the height of the interface must be checked to make sure that it does not go above the topography. The interface can be calculated everywhere, using the lower-layer potential vorticity, as in section 3b. In this case, the lower-layer potential vorticity is zero everywhere. The interface height is given by (3), and can be found by calculating the relative vorticity in the lower layer everywhere,

$$\eta = \frac{\nabla^2 \psi_2}{1 + \delta}.$$

The relative vorticity is calculated in two parts. First, the contribution from the zero potential vorticity solutions is determined analytically from the series expansion, which is equivalent to calculating η directly from the homogeneous series solution from the streamfunction in both layers. Next, the contribution from the contour integral is calculated by taking derivatives of the contour integral in the same way as in (26). For the examples discussed below, the interface does not go above the topography.

When the stratification is strong (Fig. 13a), the layers are decoupled, and the development of the contour is nearly identical to that seen in Fig. 7b, and the upper-layer response of this model is the same as the lower-layer response of the small topography model. The layer depths are equal so the fraction of the dynamically active layer taken up by the topography is the same as in the small topography example. When the stratification is weak (Fig. 13b), the layers are strongly coupled, and the amount of fluid that remains over the topography is increased, as expected from the calculation of the critical height h_{crit}. Examination of the total velocity field reveals that the shed eddy is nearly barotropic but slightly surface intensified while the flow near the topography is baroclinic (Fig. 14). This response is due to the requirement that all of the flow go around the topography in the lower layer, while some of the fluid goes over the topography in the upper layer.

The interface is depressed near the topography and raised over the eddy (Fig. 15) opposite to what is seen in the case of the small bump in the two-layer fluid (Fig. 10). A cut along the x axis shows the time evo-

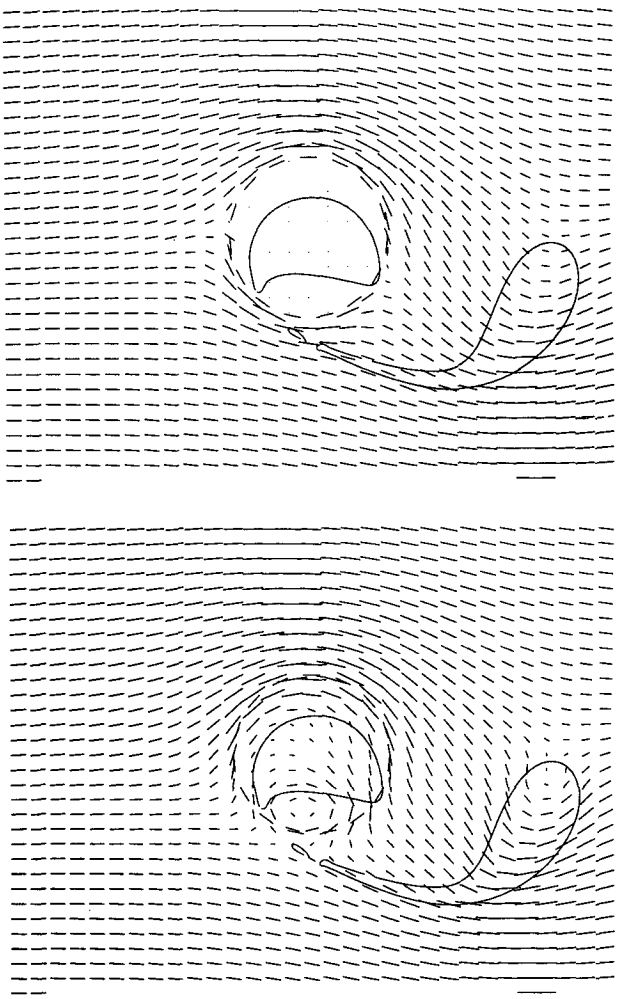

FIG. 14. Flow field for the case shown in Fig. 13b at $t = 4$: (a) lower layer and (b) upper layer.

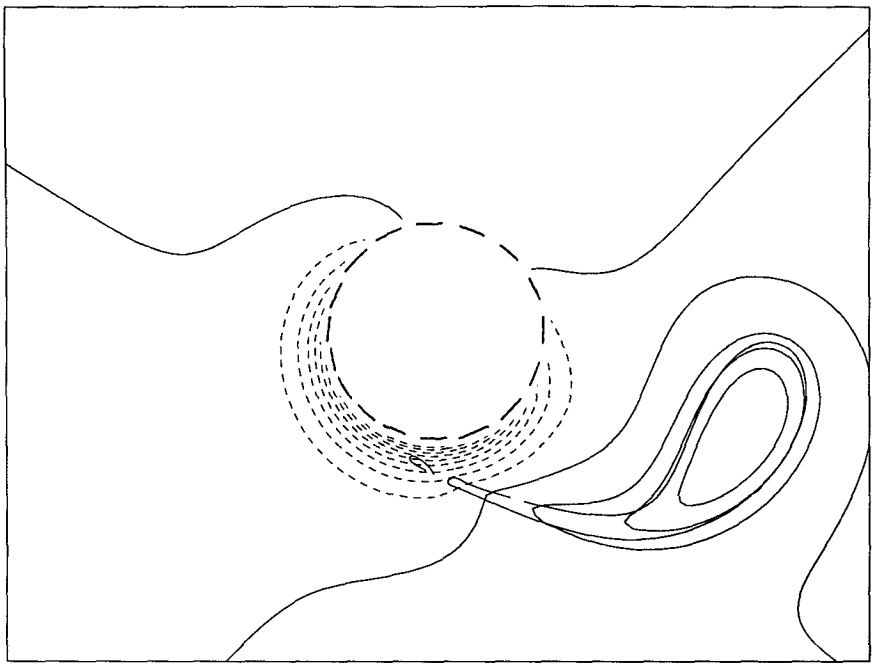

FIG. 15. Interface displacement for the case shown in Fig. 14 at $t = 4$. Dashed contours indicate negative interface displacement. The interface is depressed near the topography and is raised over the shed eddy. The shed eddy is cold core, cyclonic, and surface trapped. The solid line outside of $r = 1$ delineates fluid which originated over the topography in the upper layer.

lution of the interface (Fig. 16). As the fluid that originates over the topography moves downstream, the interface becomes depressed around the topography as it responds to the anticyclonic potential vorticity anomaly in the upper layer, and the shed eddy appears downstream of the topography as a positive perturbation as it compensates for the positive potential vorticity anomaly in the upper layer. The shed eddy is cold core because of the special structure of the stratification in this model. One would expect that the shed eddy would be cold core in a continuously stratified model only if the stratification were strong near the region of the interface, and relatively weak above that. If the fluid were strongly stratified above the interface, then the shed eddy would have a more complicated vertical structure, possibly with a cold anomaly relative to the external fluid in its deepest level and a warm anomaly in its shallowest level.

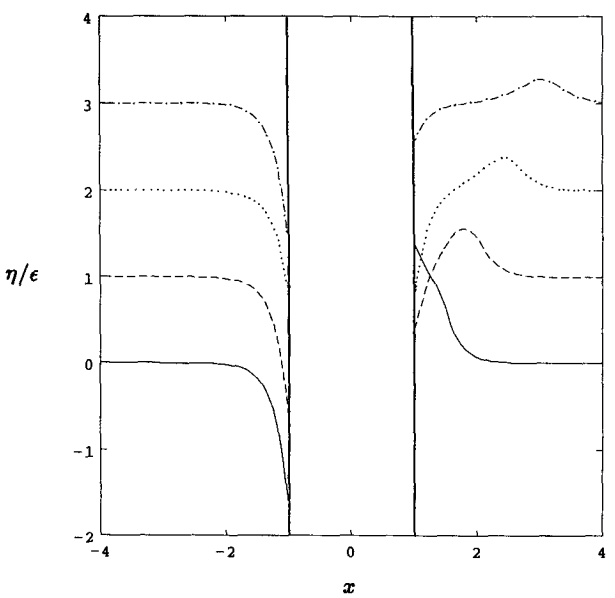

FIG. 16. Interface displacement for the case shown in Fig. 13b at a cut along the x axis at $t = 1, 2, 3, 4$. The height of the topography in the same units is 2.5. The interface is offset by 1 unit at $t = 2$, by 2 at $t = 3$, and by 3 at $t = 4$.

Examples with $\delta = 0.2$ help to illuminate the dynamics further. The potential vorticity anomaly as defined in (13) controls the qualitative evolution of the flow in the upper layer. When q_a is the same as in Fig. 13b, the development of the flow is similar to that example, even though the total topographic height is an order one amount higher (Fig. 17a). The shed eddy remains closer to the x axis as it is caught up in the islandlike flow which is important close to the topography in this example. The velocity field shows this strong islandlike flow (Fig. 18). When we let h_0 be the same as the run in Fig. 13b, more fluid is trapped over the topography because the potential vorticity anomaly is larger (Fig. 17b). The area of trapped fluid over the topography is larger in this run, but since the layer thickness is substantially less, the total volume of fluid

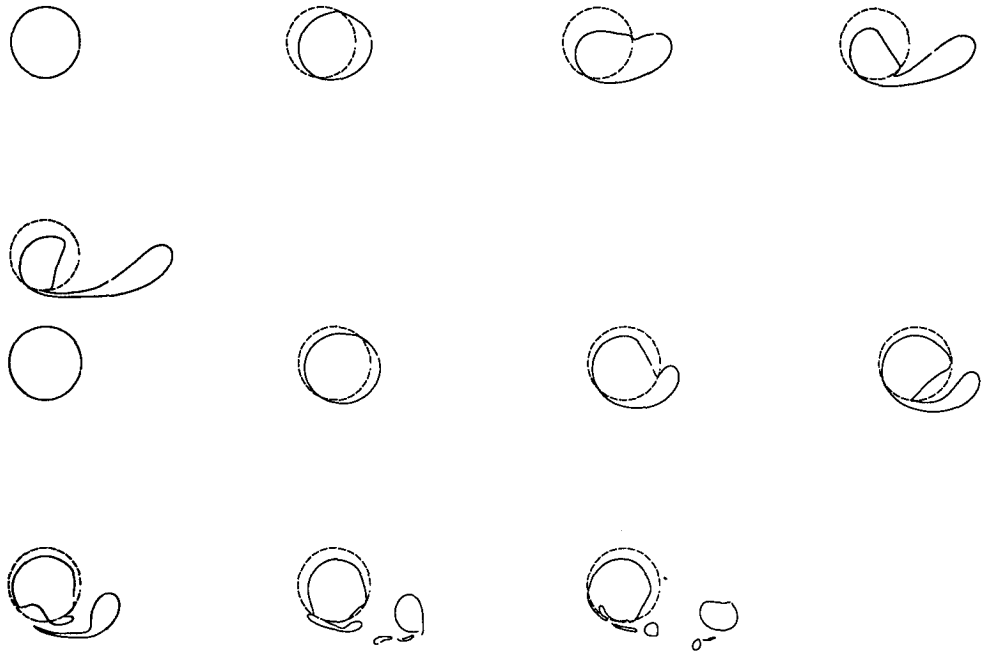

FIG. 17. Time evolution of the contour that delineates fluid which originated over the topography in the upper layer in the two-layer finite topography model for (a) $\Gamma = 4$, $\delta = 0.2$, and $h_0/\epsilon = 0.833$ at $t = 0$, 1, $\cdots$, 4 and (b) $h_0/\epsilon = 2.5$ at $t = 0$, 6.67, 13.34, $\cdots$, 40.02.

that remains over the topography is actually smaller than that in Fig. 13b.

4. Summary and conclusions

We have developed a model to study flow in a two-layer fluid when the interface intersects a boundary. Under the quasigeostrophic approximation the steady nonlinear problem reduces to a linear set of partial differential equations since the interface displacement is proportional to the difference between the upper-layer and lower-layer streamfunctions. The layer depths are constant within an order Rossby number amount so that the relative simplicity of the resulting system allows the combined effects of stratification and flow over finite topography to be considered. The model solutions are compared to one with geometry representative of what we term traditional quasigeostrophic models. Both the steady and the time-dependent solutions are studied.

From the steady solutions, two critical heights were calculated. The critical height above which closed streamlines form (h_{crit}) was considered. Higher topography leads to fluid being trapped over the topography. More fluid is trapped within closed streamlines when the stratification is weak than when it is strong, opposite to the results of the traditional model. We also determined over what range of parameters the finite depth geometry was physically consistent by calculating the height below which the interface height rises above the topography. This occurs more easily when the stratification is weak.

The model successfully combines into one the two classes of quasigeostrophic solutions that Buzzi and Speranza (1979) discussed, and the solutions contain characteristics representative of the two cases. The model predicts that the interface is depressed on the southern portion of the topography. This north–south asymmetry is due to the change in symmetry of the solution resulting from application of the boundary conditions in the lower layer. It is enhanced when positive vertical shear is included. In contrast, in traditional quasigeostrophic models the interface is uniformly raised over the topography.

The structure of the eddy that can be shed downstream in the initial value problem is not predicted from the steady solutions nor is the precise amount of the fluid trapped over the topography that originated there. To find these things out, the initial value problem was explored. The finite depth models require the development of a modified contour dynamics method. This method has more applications than those explored here (see Thompson 1990). In the traditional quasigeostrophic model, when the topography is small, the shed eddy is warm core and bottom trapped. When the topography is finite, the shed eddy is cold core and surface intensified. The steady solutions predict that less fluid is trapped near the topography as the stratification increases. In the initial value problem, this effect allows less of the fluid that originates over the topography to escape downstream. The increase of stratification has the opposite effect in the small bump model. Likewise, as the steady solutions would predict in the finite depth model, as the lower-layer depth in-

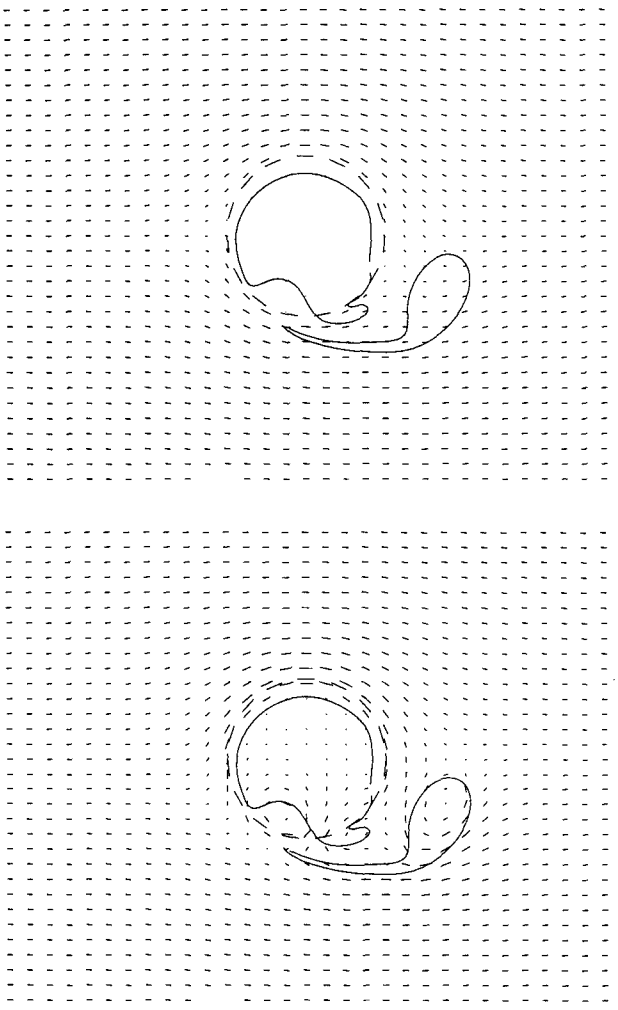

FIG. 18. Velocity field for the run shown in Fig. 17a at $t = 4$. (a) Lower-layer flow, and (b) upper-layer flow.

creases more fluid remains over the topography. The parameter that is important in determining the amount of fluid remaining trapped over the topography is the topographic height in the upper layer relative to the upper-layer thickness, the potential vorticity anomaly q_a, even when the stratification is relatively weak.

The steady solutions do not necessarily predict the exact structure of the final steady state of the initial value problem in the inviscid limit. The key assumption that allows construction of the steady solutions is that all of the fluid that originated over the topography is swept downstream. The solutions presented here show that when the background flow is relatively weak, some of the fluid originating over the topography remains trapped there. The amount of fluid that remains trapped over the topography depends not only on the stratification and strength of the background flow, but also on how the background flow is initiated (see Thompson 1990 for a further discussion). In fact, the steady solutions are only strictly correct in this context when no closed streamlines form over the topography. However, we have successfully demonstrated that the steady solutions are helpful in interpreting the results of the initial value problem.

One would like to know for what situations the finite depth model would be a good predictive tool for more complicated, continuously stratified models. Two-layer models can be calibrated according to the real oceanographic stratification (Flierl 1978), and this calibration depends on what phenomenon is of interest. Although we have not done the calibration here, we expect that the model would be most relevant to a situation in which the stratification is localized in the vertical and above that the fluid is relatively unstratified. This would happen if a seamount were to pierce the thermocline. A measure of the applicability of the two-layer model would be the scale at which motions are bottom trapped ($H_s = f_0 L/N$) versus the depth of the upper layer. If H_s is much greater than the depth of the upper layer, we would expect that our model would be relevant.

One suspects, however, that the model would not be a good approximation to a situation in which the stratification were constant, or had a slow variation with depth. To understand this, one can imagine solving the problem of continuously stratified flow impinging on a right circular cylinder. We would require that the circulation vanish below the top of the cylinder. Likewise, the streamfunction and its first derivative must be continuous at the edge of the topography. This in turn gives the requirement that only modes odd in θ can be used to construct the solution, and the component of the solution that reflects the anticyclonic vorticity over the topography no longer exists. The velocities fall off as r^{-2} in the far field as in Buzzi and Speranza (1979). In contrast, in primitive equation studies with linear stratification over smoothly varying topography, vorticity is generated near the topography through vortex stretching whenever fluid parcels move up the slope.

Acknowledgments. This research was supported by the Office of Naval Research Program N00014-90-J-1839 and comprised a portion of the author's doctoral thesis in the MIT–WHOI Joint Program in Oceanography. Additional work was done while the author was a College of Oceanography and Fisheries Sciences Fellow at the University of Washington. The author thanks Glenn Flierl for guidance in this work and Steve Meacham for sharing his contour dynamics programs.

REFERENCES

Buzzi, A., and A. Speranza, 1979: Stationary flow of quasigeostrophic, stratified atmosphere past finite amplitude obstacles. *Tellus*, **31**, 1–12.

Chapman, D. C., and D. B. Haidvogel, 1992: Formation of Taylor caps over a tall isolated seamount in a stratified ocean. *Geophys. Astrophys. Fluid Dyn.*, **64**, 31–65.

Davey, M. K., R. G. A. Hurst, and E. R. Johnson, 1992: Topographic eddies in multilayer flow. *Dyn. Atmos. Oceans.*, in press.

Flierl, G. R., 1978: Models of vertical structure and the calibration of two-layer models. *Dyn. Atmos. Oceans,* **2,** 341–381.

Gould, J. W., R. Hendry, and H. E. Huppert, 1981: An abyssal topographic experiment. *Deep-Sea Res.,* **28A,** 409–440.

Hogg, N. R., 1973: On the stratified Taylor column. *J. Fluid Mech.,* **58,** 517–537.

Huppert, H. E., and Bryan, K., 1976: Topographically generated eddies. *Deep-Sea Res.,* **23,** 655–679.

James, I. N., 1980: The forces due to geostrophic flows over shallow topography. *Geophys. Astrophys. Fluid Dyn.,* **9,** 159–177.

Janowitz, G. S., 1975: The effect of bottom topography on a stratified flow in the beta plane. *J. Geophys. Res.,* **80,** 4163–4168.

Johnson, E. R., 1977: Stratified Taylor columns on a beta-plane. *Geophys. Astrophys. Fluid Dyn.,* **9,** 159–177.

——, 1979: Finite depth stratified flow over topography on a beta-plane. *Geophys. Astrophys. Fluid Dyn.,* **12,** 35–43.

Kozlov, V. F., 1983: The method of contour dynamics in model problems of the ocean topographysical cyclogenesis. *Izv. Acad. Sci. USSR, Atmos. Oceanic Phys.,* **1983,** 635–640.

Lorenz, E. N., 1972: Barotropic instability of Rossby wave motion. *J. Atmos. Sci.,* **29,** 258–264.

Lorenz, E. N., 1972: Barotropic instability of Rossby wave motion. *J. Atmos. Sci.,* **29,** 258–264.

Meacham, S. P., 1990: Meander evolution on quasigeostrophic jets. *J. Phys. Oceanogr.,* **21,** 1139–1170.

McCartney, M. S., 1975: Inertial Taylor columns on a beta plane. *J. Fluid Mech.,* **68,** 71–95.

Merkine, L., and E. Kalnay-Rivas, 1976: Rotating stratified flow over finite isolated topography. *J. Atmos. Sci.,* **33,** 908–921.

Ou, H. W., 1991: Some effects of a seamount on oceanic flows. *J. Phys. Oceanogr.,* **21,** 1835–1845.

Polvani, L. M., 1988: Geostrophic vortex dynamics, Ph.D. thesis, Massachusetts Institute of Technology/Woods Hole Oceanographic Institute, 221 pp.

Thompson, L., 1990: *Flow over finite isolated topography.* Ph.D. thesis, Massachusetts Institute of Technology/Woods Hole Oceanographic Institute 91-05, 222 pp.

Vastano, A. C., and B. A. Warren, 1976: Perturbations to the Gulf Stream by Atlantis II Seamount. *Deep-Sea Res.,* **23,** 681–694.

Verron, J., and C. Le Provost, 1985: A numerical study of quasigeostrophic flow over isolated topography. *J. Fluid Mech.,* **154,** 231–252.